OXFORD

Cerebral Cortex, 2023, **33**, 235–245
https://doi.org/10.1093/cercor/bhac064
Advance access publication date 21 March 2022
Articles

The effect of external stimulation on functional networks in the aging healthy human brain

Anira Escrichs[1,*], Yonatan Sanz Perl[1], Noelia Martínez-Molina[1], Carles Biarnes[2,3], Josep Garre-Olmo[3,4,5], José Manuel Fernández-Real[3,4,6], Rafel Ramos[3,4,7,8], Ruth Martí[3,7,8], Reinald Pamplona[9], Ramon Brugada[3,4,10], Joaquin Serena[3,4,11], Lluís Ramió-Torrentà[3,4,11], Gabriel Coll-De-Tuero[4,7,12], Luís Gallart[13], Jordi Barretina[3], Joan C. Vilanova[2,3,4], Jordi Mayneris-Perxachs[3,6], Luca Saba[14], Salvador Pedraza[2,3,4], Morten L. Kringelbach[15,16,17], Josep Puig[2,3,4,5], Gustavo Deco[1,18,19,20,*]

[1]Computational Neuroscience Group, Center for Brain and Cognition, Department of Information and Communication Technologies, Universitat Pompeu Fabra, Barcelona, Catalonia, Spain,
[2]Department of Radiology (IDI), Hospital Universitari de Girona Dr Josep Trueta, Girona, Spain,
[3]Girona Biomedical Research Institute (IDIBGI), Hospital Universitari de Girona Dr Josep Trueta, Girona, Spain,
[4]Department of Medical Sciences, School of Medicine, University of Girona, Girona, Spain,
[5]Institut d'Assistència Sanitària, Salt, Girona, Spain,
[6]Department of Diabetes, Endocrinology and Nutrition, IDIBGI, Hospital Universitari de Girona Dr Josep Trueta, and CIBER Fisiopatología de la Obesidad y Nutrición (CIBERobn), Girona, Spain,
[7]Vascular Health Research Group of Girona (ISV-Girona), Institut Universitari d'Investigació en Atenció Primària Jordi Gol (IDIAP Jordi Gol), Girona, Spain,
[8]Primary Care Services, Catalan Institute of Health (ICS), Girona, Spain,
[9]Department of Experimental Medicine, Faculty of Medicine, University of Lleida-IRBLleida, Lleida, Spain,
[10]Cardiovascular Genetics Center, IDIBGI, CIBER-CV, Girona, Spain,
[11]Department of Neurology, Hospital Universitari de Girona Dr Josep Trueta, Girona, Spain,
[12]CIBER of Epidemiology and Public Health (CIBERESP), Madrid, Spain,
[13]Biobanc, Girona Biomedical Research Institute (IDIBGI), Girona, Spain,
[14]Department of Radiology, AOU Cagliari, University of Cagliari, Italy,
[15]Centre for Eudaimonia and Human Flourishing, University of Oxford, Oxford, UK,
[16]Department of Psychiatry, University of Oxford, Oxford, UK,
[17]Center for Music in the Brain, Department of Clinical Medicine, Aarhus University, Aarhus, Denmark,
[18]Institució Catalana de la Recerca i Estudis Avancats (ICREA), Barcelona, Catalonia, Spain,
[19]Department of Neuropsychology, Max Planck Institute for human Cognitive and Brain Sciences, Leipzig, Germany,
[20]Turner Institute for Brain and Mental Health, Monash University, Melbourne, VIC, Australia
*Corresponding author: Corresponding authors: anira.escrichs@upf.edu (AE), gustavo.deco@upf.edu (GD)

Understanding the brain changes occurring during aging can provide new insights for developing treatments that alleviate or reverse cognitive decline. Neurostimulation techniques have emerged as potential treatments for brain disorders and to improve cognitive functions. Nevertheless, given the ethical restrictions of neurostimulation approaches, *in silico* perturbation protocols based on causal whole-brain models are fundamental to gaining a mechanistic understanding of brain dynamics. Furthermore, this strategy could serve to identify neurophysiological biomarkers differentiating between age groups through an exhaustive exploration of the global effect of all possible local perturbations. Here, we used a resting-state fMRI dataset divided into middle-aged (N =310, <65 years) and older adults (N =310, ≥65) to characterize brain states in each group as a probabilistic metastable substate (PMS) space. We showed that the older group exhibited a reduced capability to access a metastable substate that overlaps with the rich club. Then, we fitted the PMS to a whole-brain model and applied *in silico* stimulations in each node to force transitions from the brain states of the older- to the middle-aged group. We found that the precuneus was the best stimulation target. Overall, these findings could have important implications for designing neurostimulation interventions for reversing the effects of aging on whole-brain dynamics.

Key words: aging; computational modeling; resting-state fMRI; brain states; *in silico* perturbations.

Introduction

Normal aging causes changes in the brain that can lead to cognitive decline, thereby affecting the quality of life and autonomy of the elderly and their caregivers (Barnes 2011; Li et al. 2015). Longitudinal studies in healthy older adults have shown an association between altered functional connectivity in resting-state and decreased cognitive functions (Persson et al. 2014; Fjell et al. 2017), thus suggesting that the resting-state could be an indicator of age-related cognitive decline. In addition, various neuroimaging studies have described that aging affects several resting-state networks (Wang et al. 2010; Ferreira and Busatto, 2013; Betzel et al. 2014; Grady et al. 2016; Spreng et al. 2016)

Received: November 19, 2021. **Revised:** January 31, 2022. **Accepted:** February 1, 2022

and the rich-club organization of the human brain (Cao et al. 2014; Zhao et al. 2015; Damoiseaux 2017; Escrichs et al. 2021a). However, a question that remains to be addressed is whether these effects could be reversed or alleviated with external stimulation protocols that promote transitions from the brain states of the older toward those observed in younger adults.

The study of causal structure-function inferences has enhanced the understanding of the mechanisms underlying human brain dynamics, both through direct neurostimulation techniques (Casali et al. 2013; Ozdemir et al. 2020) and by *in silico* stimulation protocols (Muldoon et al. 2016; Deco et al. 2018, 2019; Bolton et al. 2020; Kringelbach and Deco 2020). Noninvasive neurostimulation techniques such as transcranial electrical stimulation (tES) and transcranial magnetic stimulation (TMS) combined with neuroimaging have provided novel insights into the underlying mechanisms of stimulation-induced effects along with its impact on large-scale functional brain networks (Bestmann and Feredoes 2013). These approaches have emerged as potential treatments for neurological and neurodegenerative disorders (Fox et al. 2014; Kunze et al. 2016) as well as for improving cognitive function in healthy individuals (Clark and Parasuraman 2014). Nevertheless, experimental and ethical constraints limit the exploration of efficient practices that could be improved by the inclusion of whole-brain computational approaches along with *in silico* perturbations. In particular, dynamical models of brain activity have been fitted to different brain states to systematically apply *in silico* perturbations that promote transitions between brain states and, consequently, predict optimal neurostimulation targets (Muldoon et al. 2016; Deco et al. 2019; Ipiña et al. 2020). This strategy allows exploring dynamical brain responses elicited by controlled perturbative protocols, which are not constrained by ethical limitations (Deco et al. 2017).

In this context, we postulate that causal whole-brain modeling along with *in silico* stimulations can promote the transition between brain states of different age groups characterized by their dynamical behavior where the external stimulation represents the perturbation needed to induce that transition. The first step to finding support for this interpretation is to define the brain states associated with aging through their underlying dynamical behavior, thus providing a quantitative characterization. The probability metastable substates (PMS) space emerges as an optimal space to describe this dynamical behavior as the time evolution of a set of metastable states obtained within the Leading Eigenvector Dynamical Analysis (LEiDA) (Cabral et al. 2017; Deco et al. 2019; Kringelbach and Deco 2020). The LEiDA framework has allowed discerning brain states in depression (Figueroa et al. 2019), different states of consciousness (Deco et al. 2019; Lord et al. 2019; Kringelbach and Deco 2020; Kringelbach and Deco, 2020), and healthy aging (Cabral et al. 2017). The second step to support our hypothesis involves the transition from the older subjects' PMS representation to the youngest one induced by *in silico* perturbations. This can be done through whole-brain models, which link the underlying anatomical connectivity with functional dynamics obtained from neuroimaging data, in which the external stimulation of all brain areas can be systematically explored via *in silico* perturbations by adjusting the parameters of the model (Deco et al. 2018, 2019; Kringelbach and Deco 2020). In other words, the empirical LEiDA approach obtains the PMS of each group, whereas the model-based *in silico* approach allows us to simulate the PMS space of the older group and artificially perturb each brain area to induce transitions towards the PMS of the middle-age group. This mechanistic approach allows for an effective way of perturbing the model by simply changing the bifurcation parameter in a given brain area.

We have recently shown (Escrichs et al. 2021a) significant differences in the PMS space between older- and middle-aged healthy adults. Going radically beyond our previous work, which provided important model-free information on the differences given by the dynamics, here we used a causal whole-brain model to provide mechanistic information on how to reverse age-induced changes in dynamics. We hypothesized that a physiological differentiation of the neuronal substrate underlying the older- and middle-aged groups could be obtained by assessing, through external stimulations, the capability of each brain region to promote a transition from the brain states characterizing the older group towards the brain states characterizing the middle-aged group. Beyond the differentiation, this approach would also allow the selection of optimal stimulation targets to rebalance the underlying brain dynamics in the elderly towards more healthy states. In particular, we fit the PMS of the older group by using a causal mechanistic whole-brain model (Deco et al. 2019; Kringelbach and Deco 2020) and study exhaustively *in silico* , i.e. region by region, how to force a transition from the brain states associated with the older group to the brain states of the middle-aged group.

Materials and methods

Participants

Neuroimaging data were obtained from the Aging Imageomics Study (Puig et al. 2020) and comprised 620 healthy adults divided into two groups. The middle-aged group comprised 310 subjects aged < 65 years (mean age, 60.2±3.7 years), and the older group comprised 310 subjects aged >= 65 years (mean age, 71.8±4.5 years). We set the cut-off age based on the definition of the elderly as those people aged 65 and above (WHO 2016; United Nations, 2019). The experimental protocol was approved by the Ethics Committee of the Dr Josep Trueta University Hospital. Written informed consent was obtained from all participants. A complete description of the neuroimaging data can be consulted in Puig et al. (2020) and Escrichs et al. (2021a).

Resting-state acquisition and preprocessing

Imaging was performed on a mobile 1.5T scanner (Vantage Elan, Toshiba Medical Systems) with an 8-channel phased-array head coil with foam padding and headphones to restrict head motion and scanner noise. The high-resolution T1-weighted images were acquired with 112 slices in the axial plane (repetition time [TR] = 8 ms; echo time [TE] = 4.5 ms; flip angle = 15°; field of view (FOV) = 235 mm; and voxel size = 1.3 × 1.3 × 2.5 mm). Resting-state functional magnetic resonance imaging (fMRI) scans were acquired axially for 5 min using a gradient Echo-planar imaging (EPI) sequence (122 volumes; TR = 2500 ms; TE = 40 ms; flip angle = 83°; FOV = 230 mm; voxel size = 3.5 × 3.5 × 5 mm; no gap). Participants were asked to remain motionless as possible and close their eyes.

T1 and EPI images were automatically oriented using Conn (Whitfield-Gabrieli and Nieto-Castanon 2012). Processing Assistant for Resting-State fMRI (DPARSF) [(Chao-Gan and Yu-Feng 2010), www.rfmri.org/DPARSF], which is based on Statistical Parametric Mapping (SPM12) (http://www.fil.ion.ucl.ac.uk/spm) was used to preprocess the fMRI data. Preprocessing steps included: discarding the first 5 volumes from each scan to allow for signal stabilization; slice-timing correction; realignment for head motion correction across different volumes; T1 co-registration to the functional image; European regularisation segmentation; removal of spurious variance through linear regression: 6 parameters from the head motion correction, the white matter signal, and the cerebrospinal fluid signal using CompCor (Behzadi et al. 2007); removal of the linear trend; spatial normalization to the Montreal Neurological Institute standard space; spatial smoothing with 6-mm Full Width at Half Maximum Gaussian Kernel; and band-pass temporal filtering (0.01–0.020 Hz). Finally, the time series for each subject were extracted using a resting-state atlas of 214 nodes (Shen et al. 2013).

Difussion Tensor Imaging acquisition and preprocessing

For the whole-brain model, we used an average structural connectivity matrix (SC) from a sample of 38 unrelated healthy subjects previously described in De Filippi et al. (2021). MRI images were acquired on a 3T whole-body Siemens TRIO scanner (Hospital Clínic, Barcelona) using a dual spin-echo difussion tensor imaging (DTI) sequence (TR = 680ms; TE = 92ms; FOV = 236mm; 60 contiguous axial slices; isotropic voxel size 2 × 2 × 2 mm; no gap, and 118 × 118 matrix sizes). Diffusion was obtained with 64 optimal noncollinear diffusion directions using a single b value = 1500s/mm^2 interleaved with 9 nondiffusion b0 images. A frequency-selective fat saturation pulse was used to avoid chemical shift misregistration artifacts.

The whole-brain SC matrix was computed following the procedure applied in previous studies (Gong et al. 2009; Cao et al. 2013; Muthuraman et al. 2016; López-González et al. 2021). For each subject, a 214×214 SC was computed using the processing pipeline of the FMRIB's Diffusion Toolbox (FDT) in FMRIB's Software Library www.fmrib.ox.ac.uk/fsl. Nonbrain tissues were extracted with Brain Extraction Tool (Smith, 2002), eddy current distortions and head motion were corrected using eddy correct (Andersson and Sotiropoulos 2016), and the gradient matrix was reoriented to correct for subject motion (Leemans and Jones, 2009). Crossing fibres were modeled using BEDPOSTX, and the probability of multi-fibre orientations was computed to improve the sensitivity of nondominant fibre populations (Behrens et al. 2003, 2007). The probabilistic tractography analysis was performed for each participant in native diffusion space using PROBTRACKX. The connectivity probability SC_{np} between brain areas n and p was calculated as the total proportion of sampled fibres in all voxels in brain area n that reach any voxel in brain area p. The SC_{np} matrix was then symmetrized by computing their transpose matrix SC_{pn} and averaging both matrices. Finally, averaging the resulting matrices across all participants, a whole-brain SC matrix was obtained, representing a template of healthy adults.

Leading Eigenvector Dynamics Analysis

We characterized the empirical brain states by applying the LEiDA (Cabral et al. 2017; Deco et al. 2019; Kringelbach and Deco 2020). This analysis was described in our previous study using the same resting-state fMRI dataset (Escrichs et al. 2021a). For each participant, we filtered the time series within the narrowband 0.04–0.07 Hz (Glerean et al. 2012) and computed the Hilbert transform to obtain the phase of the BOLD signals in every time-point for all brain areas of the resting-state parcellation (Fig. 1A). Then, we computed a dynamic phase coherence connectivity matrix with size $NxNxT$, where $N=214$ is the total brain areas, and $T=117$ the total time-points. The BOLD phase coherence matrix or dynamic functional connectivity (dFC) (Fig. 1B) in each time t between each pair of brain areas n and p was estimated by computing the cosine of the phase difference as:

$$dFC(n,p,t) = \cos\left(\theta(n,t) - \theta(p,t)\right) \quad (1)$$

Given that the Hilbert Transform expresses any signal in the polar coordinate system (i.e. $x_a(t) = A(t)\cdot\cos(\varphi(t))$), applying the cosine function to brain areas n and p with similar angles at a given time t will show a phase coherence close to 1 (i.e. cos(0°)=1), whereas brain areas showing orthogonality will show a phase coherence near zero (i.e. cos(90°) = 0) (Deco et al. 2019). Second, to characterize the dFC patterns across all subjects and time-points, we obtained a leading eigenvector $V_1(t)$ for each dFC(t) at time t by capturing the dominant functional connectivity pattern rather than the whole matrices. This approach allows to reduce dimensionality on the data considerably given that only considers a $V_1(t)$ for each dynamic FC matrix. The $V_1(t)$ is a Nx1

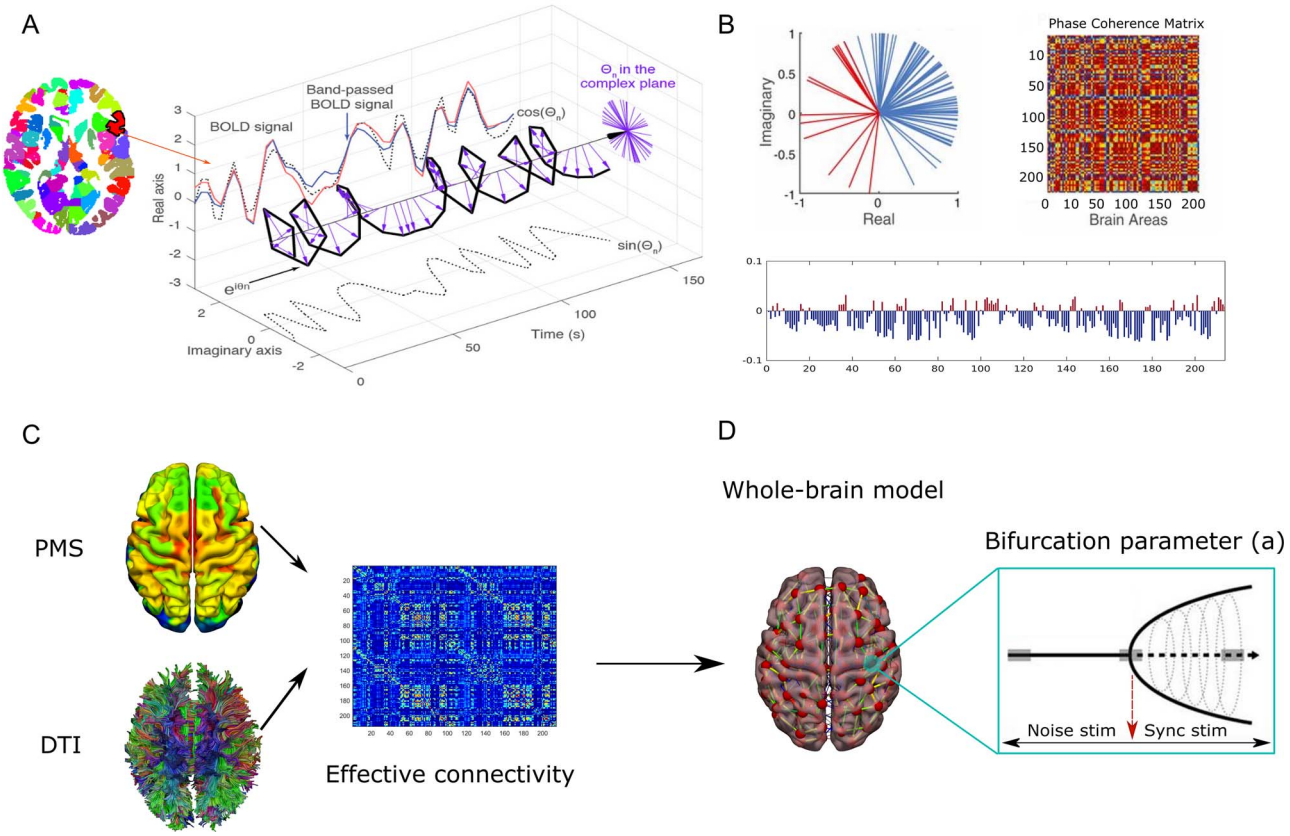

Fig. 1. PMS space, optimizing the model for whole-brain activity and *in silico* stimulations. (A) We extracted the time series using a resting-state atlas of 214 nodes and measured the Hilbert transform for each brain area. The panel shows a complex plane representing the BOLD phases for a given brain area across time. (B) Leading Eigenvector Dynamic Analysis (LEiDA) to identify dynamic functional connectivity patterns across all subjects [i.e. probabilistic metastable substates (PMS)]. The left panel shows the BOLD phases in all 214 brain areas described in the complex plane. The right panel shows the phase coherence matrix between each pair of brain areas in all time points. The vector shows the leading eigenvector $V_1(t)$, capturing the principal orientation of the BOLD phase (showing positive or negative values) for each of the 214 brain areas. (C) Whole-brain PMS model. A whole-brain dynamical model was fitted for the PMS of the older group based on the effective connectivity. (D) Stimulations *in silico* . Each brain area of the whole-brain model was systematically perturbed via *in silico* stimulations through two different protocols (noise and synchronization). The noise protocol shifts the local bifurcation parameter of each brain area to negative values, whereas the synchronization protocol shifts it to positive. Figure A and B adapted from (Deco et al. 2018; Escrichs et al. 2021a).

vector capturing the principal orientation of the BOLD phase (showing positive or negative values) for each of the 214 brain areas (Fig. 1B, lower panel). Next, we applied a k-means clustering algorithm ranged from $k = 2$ to $k = 7$ clusters to detect metastable substates or dynamic FC states from all the leading eigenvectors $V_1(t)$ across time-points, number of subjects, and groups to identify recurrent dynamic FC patterns across subjects. The total of leading eigenvectors were 117 time-points $\times$ 310 subjects $\times$ 2 groups = 72 540 $V_1(t)$. We obtained k cluster centroids, each one as an Nx1 vector representing recurrent metastable substates across all participants. The resulting k-cluster centroids define the metastable substates among which the brain dynamics are switching across time, and the probability of occurrence of each substate determines the PMS of the brain.

Whole-brain computational model

The whole-brain BOLD activity was simulated using the so-called Hopf computational model, linking the anatomy and function. The model consisted of 214 dynamical cortical and subcortical brain areas coupled with the SC matrix. The local dynamics of each brain area was described by the normal form of a supercritical Hopf bifurcation, which emulates the dynamics for each brain area from noisy to oscillatory dynamics as follows:

$$\frac{dx_n}{dt} = [a_n - x_n^2 - y_n^2]x_n - \omega_n y_n + G\sum_{p=1}^{N} C_{np}(x_p - x_n) + \beta\eta_n(t)$$
$$\frac{dy_n}{dt} = [a_n - x_n^2 - y_n^2]y_n + \omega_n x_n + G\sum_{p=1}^{N} C_{np}(y_p - y_n) + \beta\eta_n(t) \quad (2)$$

where $\eta_n(t)$ is additive Gaussian noise with standard deviation $\beta = 0.02$, and C_{np} is the SC that couples the local dynamics of brain area n with p and was normalized to a maximum value of $C = 0.2$. This normal form has a supercritical bifurcation at $a_n = 0$, such that for $a_n > 0$ the system is in a stable limit cycle oscillation with frequency $f_n = \omega_n/2\pi$, whereas for $a_n < 0$ the local dynamics are in a stable point (i.e. noisy state). The frequency ω_n of each brain area was estimated from the data that were given by the applied narrowband (i.e. $0.04 - 0.07Hz$). The variables x_n emulate the BOLD

signal of each node j. The global coupling factor G (scaled equally for each brain area) is the control parameter that allows adjusting the model to obtain the optimal dynamical working point where the simulations maximally fit the empirical data. We simulated the PMS as a function of the global coupling parameter G through the underlying SC matrix. We improved the fitting of the whole-brain model through the inclusion of the effective connectivity (EC) (Fig. 1C), where the anatomical connectivity was updated by the synaptic weights that take into account the empirical functional connectivity. The effective connections were computed by measuring the distance between the empirical $FC_{ij}^{phases\_emp}$ and the model $FC_{ij}^{phases\_mod}$ grand-averaged phase coherence matrices, and adjusted each structural connection ij separately using a gradient-descent approach. The model initially started computing with the SC matrix obtained from DTI and was run repeatedly with the updated EC matrix until the fit converged toward a stable value using the following procedure:

$$C_{ij} = C_{ij} + \epsilon \left(FC_{ij}^{phases\_emp} - FC_{ij}^{phases\_mod} \right) \quad (3)$$

where $\epsilon = 0.01$, and the grand average phase coherence matrices were defined as:

$$FC_{ij} = \left\langle \cos\left(\varphi_j(t) - \varphi_i(t) \right) \right\rangle \quad (4)$$

where $\varphi(t)$ corresponds to the BOLD signal phase (obtained by the Hilbert transform) of the brain areas j and i at time t, and the brackets correspond to the average across time.

Perturbation of the whole-brain model

The perturbation of the whole-brain model consisted of systematically perturbing the 214 brain areas of the model using two different protocols (noise and synchronization). The perturbations were based on shifting the local bifurcation parameter (a) of the optimized model (Fig. 1D). The noise (synchronization) protocol applies negative (positive) intensities to the local parameter from 0 to −0.3 (0.1).

Comparing empirical and simulated probability metastable space states

The empirical and simulated brain states were compared by using a symmetrized KL distance between the simulated and empirical probabilities as:

$$KL(P_{emp}, P_{sim}) = 0.5\left(\sum_i P_{emp}(i) \ln\left(\frac{P_{emp}(i)}{P_{sim}(i)} \right) + \sum_i P_{sim}(i) \ln\left(\frac{P_{sim}(i)}{P_{emp}(i)} \right) \right) \quad (5)$$

where $P_{emp}(i)$ are the empirical and $P_{sim}(i)$ the simulated probabilities on the same empirical extracted brain states i. The optimal simulated PMS is defined by the minimum KL distance between the empirical and simulated PMS.

Results

Leading Eigenvector Dynamics Analysis

As a proof-of-concept, we show the minimum number of clusters (k) that statistically differed between groups. In particular, the clustering configuration that best represented the resting-state data across all participants and distinguished between both groups was detected at k=3. In Figure 2A, we display the cluster centroid vectors onto the surface cortex. Interestingly, the regions of the second metastable substate showing positive values overlap with the brain's rich-club organization of the human brain (i.e. precuneus, insula, and subcortical areas, such as the caudate, putamen, hippocampus, and thalamus) (Hagmann et al. 2008; Sporns, 2013; van den Heuvel and Sporns, 2011) as found in our previous empirical study (Escrichs et al. 2021a). The probability of occurrence for the PMS of each group is shown in Fig. 2B, left panel. Specifically, the probability of the first metastable substate occurrence was higher in the older group than in the middle-age group [0.476 ± 0.008 (mean ± SE) vs. 0.453 ± 0.008 False discovery rate (FDR)-corrected, P=0.03]. By contrast, the second metastable substate's probability was higher in the middle-age group [0.288 ± 0.007 vs. 0.269 ± 0.006 in the older group, False discovery rate (FDR) P= 0.026].

Finally, we correlated the PMS values of the relevant metastable substate (i.e. rich club) with age. We found a negative correlation showing that the capability to access this state decreases while the age increases [$r(618) = -.08r, P = 0.04$]. However, even though the correlation is significant, the slope value is marginal. This result indicates the effectiveness of our method to find significant differences at the group level but not at the subject level.

Fit whole-brain computational model to the brain states of the older group

For the older group, we constructed a dynamical model of 214 nonlinear oscillators representing the macroscopic dynamical behavior of each brain area of interest (Fig. 2B, middle panel). These oscillators are coupled by a SC matrix among brain areas giving rise to collective dynamics. The local dynamics of each brain area was described by the normal form of a supercritical Hopf bifurcation, and the bifurcation parameters of each oscillator (a) were set in the edge of the bifurcation point, i.e. the optimal point to represent the metastability of brain states (Deco et al. 2017). The coupling strength parameter (G) was optimized to fit the whole-brain model to the PMS of the older group. In particular, we used the centroids of the empirical PMS of the older group and built the model based on the probability of the empirical centers. Then, we estimated the distance between the model and the empirical phase coherence matrices and adjusted

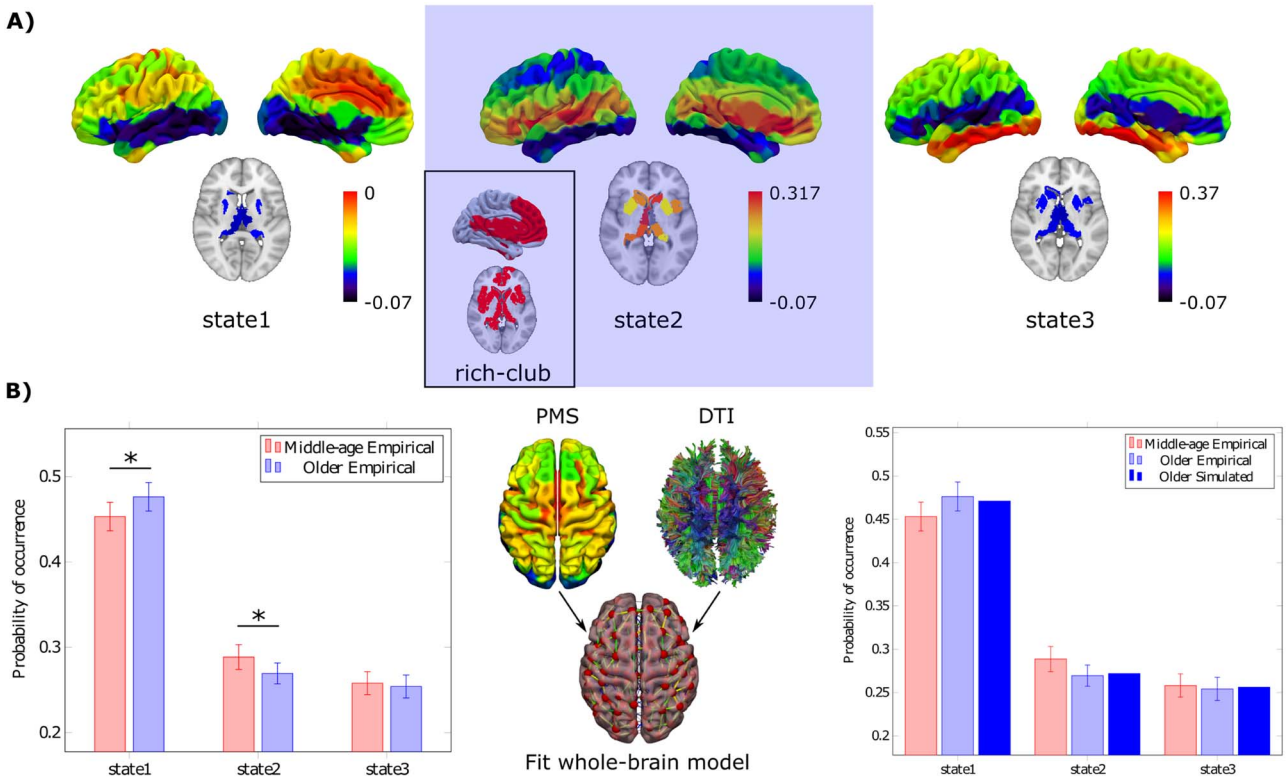

Fig. 2. Empirical PMS and whole-brain model fitting. (A) The clustering configuration that best represented our resting-state fMRI data across subjects was found for 3 states. Rendered brains show the states onto the cortex. State 1 shows negative values in all regions of the leading eigenvector. Regions showing positive values in state 2 overlap with the rich club network (precuneus, insula, caudate, putamen, hippocampus, and thalamus). State 3 was not statistically different between groups. Color bars represent the principal orientation of the BOLD phase from the leading eigenvector (showing positive o negative values). (B) The left panel shows each state and group's mean probability of occurrence, while error bars represent the 95% confidence interval. The probability of occurrence in the first state was higher in the older group. By contrast, the probability of occurrence in the second state was higher in the middle-age group. The whole-brain model was fitted to the empirical PMS of the older group (middle panel). The right panel shows the resulting model (electric blue), remarkably similar to their empirical version (blue). P-values are based on Monte-Carlo permutation tests, ∗ represents $P<0.05$.

each structural connection separately using a gradient-descent algorithm. The model was run repeatedly with the updated EC until convergence to a stable point. We tested the differences between the empirical and the simulated probabilities by computing the symmetrized Kullback–Leibler (KL) distance (see Material and methods). The optimal working point of the model was found at G=0.02, i.e. where the model fits the empirical PMS data of the older group. The generated model reached an excellent fit between the empirical and the simulated probabilities (Fig. 2B, right panel).

In silico stimulations to force transitions between brain states

We applied two different stimulation protocols (i.e. noise and synchronization) in order to force transitions from the PMS of the older group to the PMS of the middle-aged group. In Figure 3A, we show the schematic procedure to force transitions between brain states. Specifically, we started from the simulated PMS that presented the highest similarity to the empirical PMS of the older group and perturbed the model to force the transition to the empirical PMS of the middle-age group. The stimulation protocols were based on systematically shifting the local bifurcation parameter (a) of the optimized whole-brain model. The noise protocol applies negative intensities to the local parameter, whereas the synchronization applies positive intensities. The strength of the perturbation is linked to the shifting of the local bifurcation parameter. Concretely, we systematically perturbed each of the 214 brain areas of the whole-brain model and compared the distributions with the empirical PMS of the middle-age group. The optimal perturbation is that yields that the first brain state decreases, the second increases and the third brain state remains similar (Fig. 3A, right panel).

Our results show that the KL distances between the empirical PMS of the middle-aged group and the perturbed model were minimal in some brain areas for the noise protocol, and thus a good transition between brain states was obtained (Fig. 3B, left panel). The potential brain areas to achieve a good transition between brain states were the precuneus and lingual gyrus, bilateral middle temporal gyrus, bilateral calcarine sulcus, bilateral inferior gyrus orbitofrontal part, left superior temporal gyrus, left insula, bilateral putamen, bilateral thalamus, and right caudate (Fig. 3B, middle panel). In contrast, the KL distances were higher in the synchronization protocol for all perturbation strengths

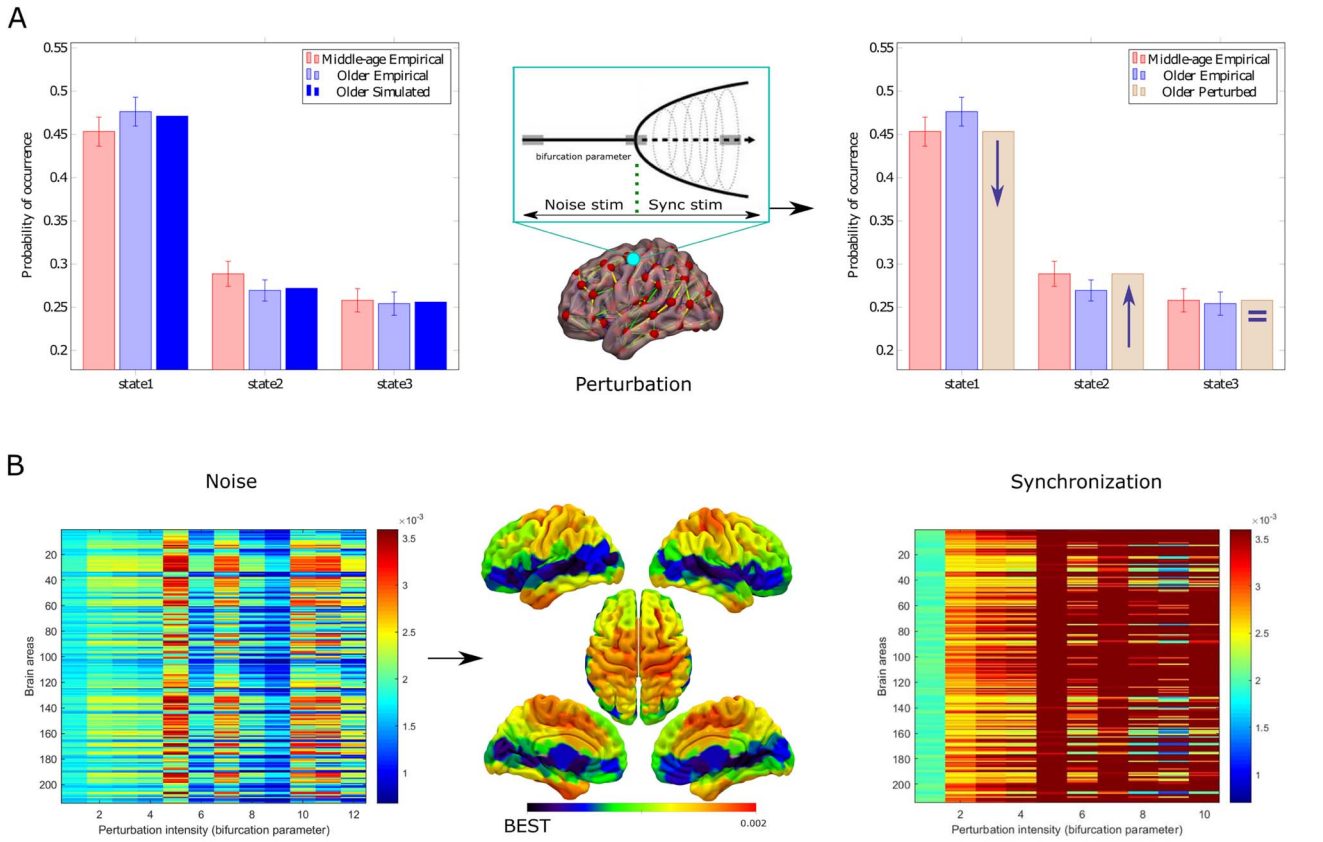

Fig. 3. Noise and synchronization stimulation protocols. (A) Forcing transitions from the model of the older group (electric blue) to the empirical PMS of the middle-age group (red). The whole-brain model was perturbed at the optimal working point using two different protocols (noise and synchronization), which shifted the local bifurcation parameter to negative and positive values, respectively (middle panel). The optimal perturbation is that which achieves the first state decreases, the second state increases, and the third state remains similar (right panel). (B) The left matrix shows the KL-distance value after applying the noise protocol's perturbation intensity (from softer to stronger) in each brain area. This protocol presented the best effectiveness since KL distances were minimal in some brain areas. The brain rendered onto the cortex shows that the optimal brain areas to induce the transitions were the precuneus and lingual gyrus, bilateral middle temporal gyrus, bilateral calcarine sulcus, bilateral inferior gyrus orbitofrontal part, left superior temporal gyrus, left insula, bilateral putamen, bilateral thalamus, and right caudate. The color scale represents the KL distance between the PMS of the middle-age group and the perturbed model using the noise protocol. The right matrix shows that the synchronization protocol presented poor effectiveness given that KL distances were longer than in the noise protocol.

and perturbed brain areas (Fig. 3B, right panel). This result indicates the unsuitability of the synchronization protocol to force the transition.

Finally, in Figure 4 we display the PMS comparison between empirical, modeled, and perturbation conditions. We show the best transition and the worst transition after the perturbation. It is noticeable that after perturbing the precuneus, the probabilities of the empirical PMS of the middle-aged group and perturbed model of the older group are almost the same for the three metastable substates considered (the KL distance was minimal). By contrast, the worst target was the postcentral gyrus, since the probabilities of the states barely changed after the perturbation. These results suggest that the right precuneus is the brain area that induces the best effective transition between brain states.

Discussion

In this work, we used empirical and computational approaches to study the causal dynamical mechanisms allowing the transition between brain states of different age groups. Our empirical approach identified that the older group has a lower probability of accessing a state that overlaps with the rich club. Then, we investigated the effect of perturbing all brain areas to induce optimal transitions from the states of the older aged group to the states of the middle-aged group by using causal whole-brain modeling and *in silico* perturbations. These results illustrated that forcing a shift in the intrinsic local dynamics of the right precuneus and other brain areas belonging to the rich club (insula, putamen, caudate, and thalamus) is suitable for inducing those transitions. Crucially, our model-based *in silico* approach provides causal evidence that external stimulations in specific local brain areas can reshape whole-brain dynamics in the aging brain. Importantly, this could provide new insights into the differential sensitivity of each brain area to *in silico* perturbations as a specific model-based biomarker relating local activity with global brain dynamics.

Understanding the underlying brain changes occurring during normal aging can contribute to develop ing treatments to reverse cognitive impairment. In this regard, Noninvasive neurostimulation therapies stand as a promising intervention for brain disorders (Clark and Parasuraman 2014; Kunze et al. 2016). Nevertheless,

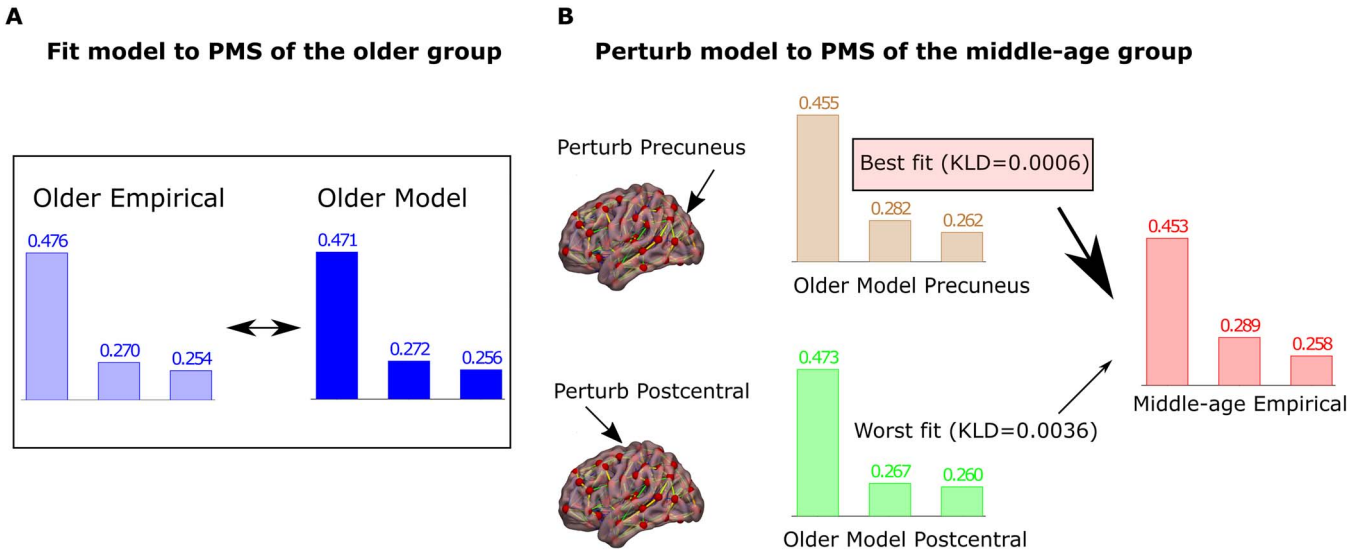

Fig. 4. PMS comparison between empirical, modeled, and perturbation conditions. (A) Comparison between the probability of occurrence of the empirical and modeled PMS of the older group. (B) We show the best and worst transitions after the perturbation. These results clearly show an optimal transition from the perturbed model towards the PMS of the middle-aged group after changing the bifurcation parameter of the right precuneus with the noise protocol. In particular, this perturbation decreased the probability of occurrence of the first state, increased the probability of the second, and kept the probability of the third similar. By contrast, the postcentral gyrus shows a non-optimal transition since the states' probabilities barely changed after the perturbation.

there are two different but related limitations for the application of such treatments. The first refers to the lack of a consensual definition of a brain state capable of being quantitatively characterized that differentiates the activity of an older from a younger brain. The second issue concerns the limitations to exploring the vast space of possible interventions due to experimental and ethical constraints (Deco et al. 2017). Here, we addressed these 2 issues by applying whole-brain computational models, which allowed us to systematically explore brain responses elicited by *in silico* perturbations of fMRI empirical data of healthy older and middle-aged subjects.

We tested the hypothesis that causal modeling could predict optimal stimulation targets to rebalance the underlying brain dynamics in the elderly. Interestingly, we show that this approach can predict optimal targets to force transitions between brain states of different ages. Previous experimental studies investigated the effects of localized external perturbations during states of reduced awareness in humans (Angelakis et al. 2014; Thibaut et al. 2014; Zhang et al. 2019) and mild cognitive impairment (Hampstead et al. 2017). However, the systematic exploration via perturbations of all brain areas of the human brain can only be performed through computational models that simulate the underlying brain activity (Spiegler et al. 2016). In this direction, recent works have implemented whole-brain models and *in silico* perturbations to explore the elicited responses from external stimulations in different brain states such as sleep, anesthesia, disorders of consciousness and even in altered states such as meditation or the psychedelic state (Deco et al. 2019; Ipiña et al. 2020; Kringelbach et al. 2020; Sanz Perl et al. 2021; Escrichs et al. 2021b).

Our empirical approach using LEiDA identified PMS differences between older and middle-age groups. In particular, we found differences in a state that closely overlaps with the so-called rich club (Hagmann et al. 2008; van den Heuvel and Sporns, 2011; Sporns, 2013), that in turn, the rich club overlaps with the Default mode network (DMN) (van den Heuvel and Sporns, 2011; Damoiseaux 2017). Our results reveal that, compared with middle-aged subjects, older subjects showed a lower probability of occurrence of this state that can be interpreted as an alteration in the intrinsic dynamics within the rich-club or damage in any of their brain areas involved (Escrichs et al. 2021a). In line with this finding, recent studies have suggested that the alterations in brain dynamics observed in the elderly could be due to a deficiency in the rich-club organization (Cao et al. 2014; Zhao et al. 2015; Damoiseaux 2017). This framework demonstrates that the brain spatiotemporal dynamic, summarized in the PMS, provides crucial information to characterize different aged groups. Furthermore, this result could be related to Northoff and colleagues' proposal about spatiotemporal neuroscience and the common currency between brain and mind (Northoff et al. 2020).

Our model-based *in silico* approach allowed us to test the effectiveness of 2 different stimulation protocols named noise and synchronization. The noise protocol reduces the value of the bifurcation parameter of the stimulated node resulting in noise outweighing oscillatory behavior, whereas the synchronization protocol yields the opposite effect. The fact that the noise protocol

leads to better results means that the local bifurcation parameters must be mostly below or at the edge of bifurcation, thus favoring the local dynamics in the most susceptible regime. Furthermore, this result could be related to brain overactivation that has been largely documented in the elderly. Particularly, older adults show overactivation in frontal brain areas (Davis et al. 2008; Reuter-Lorenz and Cappell, 2008; Cabeza et al. 2018; Yao and Hsieh 2021), and among resting-state networks (Betzel et al. 2014; Geerligs et al. 2015; Spreng et al. 2016; Escrichs et al. 2021a). Thus, one possible mechanism could be that noise stimulation decreases these functional overactivations.

Interestingly, the results show that the brain area that promoted the best transition between brain states was the precuneus. The precuneus plays a central functional role in the DMN (Utevsky et al. 2014) and is involved in complex functions like memory, perception, mental imagery, and responses to pain (Cavanna and Trimble 2006). Furthermore, we found that the other brain areas that promoted an excellent transition are part of the so-called rich club (i.e. the precuneus, insula, putamen, caudate, and thalamus) (van den Heuvel and Sporns, 2011; Van Den Heuvel et al. 2012). Evidence suggests that a disruption in one of these regions can affect network efficiency and global brain function (van den Heuvel and Sporns, 2011).

Lastly, we would like to acknowledge some limitations in the study. One inherent limitation is related to using a cross-sectional approach that, by definition, cannot measure individual changes in brain dynamics. The image acquisition protocol with TR also limits this work = 2.5s in a 1.5T scanner. A protocol with increased spatial and temporal resolution could allow a more accurate representation of the underlying brain dynamics. Furthermore, we did not correlate our empirical PMS results with behavioral or cognitive measures. Future studies could explore the relationship between cognitive assessments with brain dynamics for more clinical relevance. Another limitation concerns the parcellation used, which was based on an atlas of 214 nodes. Using brain atlases with a large number of nodes could produce results with better local sensitivity.

Overall, the model-based *in silico* approach provides causal evidence that external stimulations in specific local brain areas can reshape whole-brain dynamics in aging. From a clinical standpoint, the methods and results presented here suggest optimal targets for neurostimulation techniques to induce transitions toward a healthy regime. This framework could improve the diagnosis, prognosis, and therapeutic responsiveness of aging effects in healthy adults and other conditions such as neuropsychiatry diseases and disorders of consciousness.

Acknowledgments

AE, YS and GD were supported by the HBP SGA3 Human Brain Project Specific Grant Agreement 3 (grant agreement no. 945539), funded by the EU H2020 FET Flagship.

Conflict of interest statement. None declared.

References

Andersson JL, Sotiropoulos SN. An integrated approach to correction for off-resonance effects and subject movement in diffusion MR imaging. *NeuroImage*. 2016:125:1063–1078.

Angelakis E, Liouta E, Andreadis N, Korfias S, Ktonas P, Stranjalis G, Sakas DE. Transcranial direct current stimulation effects in disorders of consciousness. *Arch Phys Med Rehabil*. 2014:95:283–289.

Barnes CA. Secrets of aging: what does a normally aging brain look like? *F1000 Biol Rep*. 2011:3:22.

Behrens T, Woolrich M, Jenkinson M, Johansen-Berg H, Nunes R, Clare S, Matthews P, Brady J, Smith S. Characterization and propagation of uncertainty in diffusion-weighted MR imaging. *Magn Reson Med*. 2003:50:1077–1088.

Behrens TEJ, Berg HJ, Jbabdi S, Rushworth MFS, Woolrich MW. Probabilistic diffusion tractography with multiple fibre orientations: What can we gain? *NeuroImage*. 2007:34:144–155.

Behzadi Y, Restom K, Liau J, Liu TT. A component based noise correction method (CompCor) for BOLD and perfusion based fMRI. *NeuroImage*. 2007:37:90–101.

Bestmann S, Feredoes E. Combined neurostimulation and neuroimaging in cognitive neuroscience: Past, present, and future. *Ann N Y Acad Sci*. 2013:1296:11–30.

Betzel RF, Byrge L, He Y, Goñi J, Zuo XNN, Sporns O. Changes in structural and functional connectivity among resting-state networks across the human lifespan. *NeuroImage*. 2014:102:345–357.

Bolton TA, Morgenroth E, Preti MG, Van De Ville D. Tapping into Multi-Faceted Human Behavior and Psychopathology Using fMRI Brain Dynamics. *Trends Neurosci*. 2020:43:667–680.

Cabeza R, Albert M, Belleville S, Craik FI, Duarte A, Grady CL, Lindenberger U, Nyberg L, Park DC, Reuter-Lorenz PA, et al. Maintenance, reserve and compensation: the cognitive neuroscience of healthy ageing. *Nat Rev Neurosci*. 2018:19:701–710.

Cabral J, Vidaurre D, Marques P, Magalhães R, Silva Moreira P, Miguel Soares J, Deco G, Sousa N, Kringelbach ML. Cognitive performance in healthy older adults relates to spontaneous switching between states of functional connectivity during rest. *Sci Rep*. 2017:7:5135.

Cao Q, Shu N, An L, Wang P, Sun L, Xia MR, Wang JH, Gong GL, Zang YF, Wang YF, et al. Probabilistic diffusion tractography and graph theory analysis reveal abnormal white matter structural connectivity networks in drug-naive boys with attention deficit/hyperactivity disorder. *J Neurosci*. 2013:33:10676–10687.

Cao M, Wang JHH, Dai ZJJ, Cao XYY, Jiang LLL, Fan FMM, Song XWW, Xia MRR, Shu N, Dong Q, et al. Topological organization of the human brain functional connectome across the lifespan. *Dev Cogn Neurosci*. 2014:7:76–93.

Casali AG, Gosseries O, Rosanova M, Boly M, Sarasso S, Casali KR, Casarotto S, Bruno MA, Laureys S, Tononi G, et al. A theoretically based index of consciousness independent of sensory processing and behavior. *Sci Transl Med*. 2013:5:198ra105–198ra105.

Cavanna AE, Trimble MR. The precuneus: a review of its functional anatomy and behavioural correlates. *Brain*. 2006:129:564–583.

Chao-Gan Y, Yu-Feng Z. DPARSF: A MATLAB toolbox for "pipeline" data analysis of resting-state fMRI. *Front Syst Neurosci*. 2010:4:13.

Clark VP, Parasuraman R. Neuroenhancement: enhancing brain and mind in health and in disease. *NeuroImage*. 2014:85:889–894.

Damoiseaux JS. Effects of aging on functional and structural brain connectivity. *NeuroImage*. 2017:160:32–40.

Davis SW, Dennis NA, Daselaar SM, Fleck MS, Cabeza R. Que PASA? The posterior-anterior shift in aging. *Cereb Cortex*. 2008:18: 1201–1209.

De Filippi E, Escrichs A, Càmara E, Garrido C, Sánchez-Fibla M, Gilson M, Deco G. Meditation-induced effects on whole-brain structural and effective connectivity. *bioRxiv*. 2021 June:10.447903.

Deco G, Kringelbach ML, Jirsa VK, Ritter P. The dynamics of resting fluctuations in the brain: metastability and its dynamical cortical core. *Sci Rep*. 2017:7:3095.

Deco G, Cabral J, Saenger VM, Boly M, Tagliazucchi E, Laufs H, Van Someren E, Jobst B, Stevner A, Kringelbach ML. Perturbation of whole-brain dynamics *in silico* reveals mechanistic differences between brain states. *NeuroImage*. 2018:169:46–56.

Deco G, Cruzat J, Cabral J, Tagliazucchi E, Laufs H, Logothetis NK, Kringelbach ML. Awakening: predicting external stimulation to force transitions between different brain states. *Proc Natl Acad Sci*. 2019:116:18088–18097.

Escrichs A, Biarnes C, Garre-Olmo J, Fernández-Real JM, Ramos R, Pamplona R, Brugada R, Serena J, Ramió-Torrentà L, Coll-De-Tuero G, et al. Whole-brain dynamics in aging: disruptions in functional connectivity and the role of the rich club. *Cereb Cortex*. 2021a:31:2466–2481.

Escrichs A, Perl YS, Uribe C, Camara E, Türker B, Pyatigorskaya N, López-González A, Pallavicini C, Panda R, Annen J, et al. Unifying turbulent dynamics framework distinguishes different brain states. *bioRxiv*. 2021b:14.464380.

Ferreira LK, Busatto GF. Resting-state functional connectivity in normal brain aging. *Neurosci Biobehav Rev*. 2013:37:384–400.

Figueroa CA, Cabral J, Mocking RJT, Rapuano KM, van Hartevelt TJ, Deco G, Expert P, Schene AH, Kringelbach ML, Ruhé HG. Altered ability to access a clinically relevant control network in patients remitted from major depressive disorder. *Hum Brain Mapp*. 2019:40:2771–2786.

Fjell AM, Sneve MH, Grydeland H, Storsve AB, Walhovd KB. The disconnected brain and executive function decline in aging. *Cereb Cortex*. 2017:27:2303–2317.

Fox MD, Buckner RL, Liu H, Chakravarty MM, Lozano AM, Pascual-Leone A. Resting-state networks link invasive and noninvasive brain stimulation across diverse psychiatric and neurological diseases. *Proc Natl Acad Sci*. 2014:111:E4367–E4375.

Geerligs L, Renken RJ, Saliasi E, Maurits NM, Lorist MM. A brain-wide study of age-related changes in functional connectivity. *Cereb Cortex*. 2015:25:1987–1999.

Glerean E, Salmi J, Lahnakoski JM, Jääskeläinen IP, Sams M. Functional magnetic resonance imaging phase synchronization as a measure of dynamic functional connectivity. *Brain Connect*. 2012:2:91–101.

Gong G, Rosa-Neto P, Carbonell F, Chen ZJ, He Y, Evans AC. Age- and gender-related differences in the cortical anatomical network. *J Neurosci*. 2009:29:15684–15693.

Grady C, Sarraf S, Saverino C, Campbell K. Age differences in the functional interactions among the default, frontoparietal control, and dorsal attention networks. *Neurobiol Aging*. 2016:41:159–172.

Hagmann P, Cammoun L, Gigandet X, Meuli R, Honey CJ, Wedeen VJ, Sporns O. Mapping the structural core of human cerebral cortex. *PLoS Biol*. 2008:6:e159.

Hampstead BM, Sathian K, Bikson M, Stringer AY. Combined mnemonic strategy training and high-definition transcranial direct current stimulation for memory deficits in mild cognitive impairment. Alzheimer's dement. *Transl Res Clin Interv*. 2017:3:459–470.

van den Heuvel MP, Sporns O. Rich-club organization of the human connectome. *J Neurosci*. 2011:31:15775–15786.

Ipiña IP, Kehoe PD, Kringelbach M, Laufs H, Ibañez A, Deco G, Perl YS, Tagliazucchi E. Modeling regional changes in dynamic stability during sleep and wakefulness. *NeuroImage*. 2020:215:116833.

Kringelbach ML, Deco G. Brain states and transitions: insights from computational neuroscience. *Cell Rep*. 2020:32:108128.

Kringelbach ML, Cruzat J, Cabral J, Knudsen GM, Carhart-Harris R, Whybrow PC, Logothetis NK, Deco G. Dynamic coupling of whole-brain neuronal and neurotransmitter systems. *Proc Natl Acad Sci U S A*. 2020:117:9566–9576.

Kunze T, Hunold A, Haueisen J, Jirsa V, Spiegler A. Transcranial direct current stimulation changes resting state functional connectivity: a large-scale brain network modeling study. *NeuroImage*. 2016:140:174–187.

Leemans A, Jones DK. The B -matrix must be rotated when correcting for subject motion in DTI data. *Magn Reson Med*. 2009:61:1336–1349.

Li HJ, Hou XH, Liu HH, Yue CL, Lu GM, Zuo XN. Putting age-related task activation into large-scale brain networks: a meta-analysis of 114 fMRI studies on healthy aging. *Neurosci Biobehav Rev*. 2015:57:156–174.

López-González A, Panda R, Ponce-Alvarez A, Zamora-López G, Escrichs A, Martial C, Thibaut A, Gosseries O, Kringelbach ML, Annen J, et al. Loss of consciousness reduces the stability of brain hubs and the heterogeneity of brain dynamics. *Commun Biol*. 2021:4:1–15.

Lord LDD, Expert P, Atasoy S, Roseman L, Rapuano K, Lambiotte R, Nutt DJ, Deco G, Carhart-Harris RL, Kringelbach ML, et al. Dynamical exploration of the repertoire of brain networks at rest is modulated by psilocybin. *NeuroImage*. 2019:199:127–142.

Muldoon S, Pasqualetti F, Gu S, Cieslak M, Grafton ST, Vettel JM. Stimulation-based control of dynamic brain networks. *PLoS Comput Biol*. 2016:12:1005076.

Muthuraman M, Fleischer V, Kolber P, Luessi F, Zipp F, Groppa S. Structural brain network characteristics can differentiate CIS from early RRMS. *Front Neurosci*. 2016:10:14.

Northoff G, Wainio-Theberge S, Evers K. Is temporo-spatial dynamics the "common currency" of brain and mind? in quest of "spatiotemporal neuroscience". *Phys Life Rev*. 2020:33:34–54.

Ozdemir RA, Tadayon E, Boucher P, Momi D, Karakhanyan KA, Fox MD, Halko MA, Pascual-Leone A, Shafi MM, Santarnecchi E. Individualized perturbation of the human connectome reveals reproducible biomarkers of network dynamics relevant to cognition. *Proc Natl Acad Sci*. 2020:117:8115–8125.

Persson J, Pudas S, Nilsson LG, Nyberg L. Longitudinal assessment of default-mode brain function in aging. *Neurobiol Aging*. 2014:35:2107–2117.

Puig J, Biarnes C, Pedraza S, Vilanova JC, Pamplona R, Fernández-Real JM, Brugada R, Ramos R, Coll-de Tuero G, Calvo-Perxas L, et al. The aging imageomics study: rationale, design and baseline characteristics of the study population. *Mech Ageing Dev*. 2020:189:111257.

Reuter-Lorenz PA, Cappell KA. Neurocognitive aging and the compensation hypothesis. *Curr Dir Psychol Sci*. 2008:17:177–182.

Sanz Perl Y, Pallavicini C, Pérez Ipiña I, Demertzi A, Bonhomme V, Martial C, Panda R, Annen J, Ibañez A, Kringelbach M, et al. Perturbations in dynamical models of whole-brain activity dissociate between the level and stability of consciousness. *PLoS Comput Biol*. 2021:17:e1009139.

Shen X, Tokoglu F, Papademetris X, Constable RT. Groupwise whole-brain parcellation from resting-state fMRI data for network node identification. *NeuroImage*. 2013:82:403–415.

Smith SM. Fast robust automated brain extraction. *Hum Brain Mapp*. 2002:17:143–155.

Spiegler A, Hansen EC, Bernard C, McIntosh AR, Jirsa VK. Selective activation of resting-state networks following focal stimulation in a connectome-based network model of the human brain. *Eneuro*. 2016:3:5.

Sporns O. Network attributes for segregation and integration in the human brain. *Curr Opin Neurobiol*. 2013:23:162–171.

Spreng RN, Stevens WD, Viviano JD, Schacter DL. Attenuated anticorrelation between the default and dorsal attention networks with aging: evidence from task and rest. *Neurobiol Aging*. 2016:45:149–160.

Thibaut A, Bruno MA, Ledoux D, Demertzi A, Laureys S. TDCS in patients with disorders of consciousness: Sham-controlled randomized double-blind study. *Neurology*. 2014:82:1112–1118.

United Nations. *World population ageing 2019*. United Nations: Technical report; 2019

Utevsky AV, Smith DV, Huettel SA. Precuneus is a functional core of the default-mode network. *J Neurosci*. 2014:34:932–940.

Van Den Heuvel MP, Kahn RS, Goñi J, Sporns O. High-cost, high-capacity backbone for global brain communication. *Proc Natl Acad Sci*. 2012:109:11372–11377.

Wang L, LaViolette P, O'Keefe K, Putcha D, Bakkour A, Van Dijk KR, Pihlajamäki M, Dickerson BC, Sperling RA. Intrinsic connectivity between the hippocampus and posteromedial cortex predicts memory performance in cognitively intact older individuals. *NeuroImage*. 2010:51:910–917.

Whitfield-Gabrieli S, Nieto-Castanon A. Conn : a functional connectivity toolbox for correlated and anticorrelated brain networks. *Brain Connect*. 2012:2:125–141.

WHO. WHO | Proposed working definition of an older person in Africa for the MDS Project. *World Heal Organ*. 2016. https://www.who.int/healthinfo/survey/ageingdefnol.

Yao ZF, Hsieh S. Age differences of the hierarchical cognitive control and the frontal rostro-caudal functional brain activation. *Cereb Cortex*. 2021:1–19.

Zhang D, Li H, Sun J, Hu W, Jin W, Li S, Tong S. Antidepressant-like effect of low-intensity transcranial ultrasound stimulation. *IEEE Trans Biomed Eng*. 2019:66:411–420.

Zhao T, Cao M, Niu H, Zuo XN, Evans A, He Y, Dong Q, Shu N. Age-related changes in the topological organization of the white matter structural connectome across the human lifespan. *Hum Brain Mapp*. 2015:36:3777–3792.